Received: 23 February 2021 | Revised: 14 September 2021 | Accepted: 19 September 2021 | Published on: 29 October 2021

DOI: 10.1002/joc.7404

RESEARCH ARTICLE

International Journal of Climatology RMetS

Evaluation of onset, cessation and seasonal precipitation of the Southeast Asia rainy season in CMIP5 regional climate models and HighResMIP global climate models

Mugni Hadi Hariadi[1,2,3] | **Gerard van der Schrier**[1] | **Gert-Jan Steeneveld**[2] | **Ardhasena Sopaheluwakan**[3] | **Albert Klein Tank**[2,4] | **Malcolm John Roberts**[4] | **Marie-Pierre Moine**[5] | **Alessio Bellucci**[6] | **Retish Senan**[7] | **Etienne Tourigny**[8] | **Dian Putrasahan**[9]

[1]Royal Netherlands Meteorological Institute (KNMI), De Bilt, Netherlands

[2]Meteorology and Air Quality (MAQ) Section, Wageningen University, Wageningen, Netherlands

[3]Indonesian Agency for Meteorology, Climatology and Geophysics (BMKG), Jakarta, Indonesia

[4]Met Office Hadley Centre for Climate Science and Services, Exeter, UK

[5]CECI, Université de Toulouse, CERFACS/CNRS, Toulouse, France, Toulouse, France

[6]Euro-Mediterranean Center on Climate Change (CMCC), Lecce, Italy

[7]European Centre for Medium Range Weather Forecasts (ECMWF), Reading, UK

[8]Barcelona Supercomputing Centre (BSC), Barcelona, Spain

[9]Max Planck Institute for Meteorology (MPI-M), Hamburg, Germany

Correspondence
Mugni Hadi Hariadi, Royal Netherlands Meteorological Institute (KNMI), Utrechtseweg 297, De Bilt 3731 GA, Netherlands.
Email: mugni.hariadi@knmi.nl; mugni1.hariadi@wur.nl

Funding information
Indonesia Endowment Fund for Education (LPDP), Grant/Award Number: S-353/LPDP.3/2019; H2020 Marie Skłodowska-Curie, Grant/Award Number: 748750; European Union's Horizon 2020 Research and Innovation Programme, Grant/Award Number: 641727

Abstract

Representing the rainy season of the maritime continent is a challenge for global and regional climate models. Here, we compare regional climate models (RCMs) based on the coupled model intercomparison project phase 5 (CMIP5) model generation with high-resolution global climate models with a comparable spatial resolution from the HighResMIP experiment. The onset and the total precipitation of the rainy season for both model experiments are compared against observational datasets for Southeast Asia. A realistic representation of the monsoon rainfall is essential for agriculture in Southeast Asia as a delayed onset jeopardizes the possibility of having three annual crops. In general, the coupled historical runs (Hist-1950) and the historical force atmosphere run (HighresSST) of the high-resolution model intercomparison project (HighResMIP) suite were consistently closer to the observations than the RCM of CMIP5 used in this study. We find that for the whole of Southeast Asia, the HighResMIP models simulate the onset date and the total precipitation of the rainy season over the region closer to the observations than the other model sets used in this study. High-resolution models in the HighresSST experiment showed a similar performance to their low-resolution equivalents in simulating

the monsoon characteristics. The HighresSST experiment simulated the anomaly of the onset date and the total precipitation for different El Niño-southern oscillation conditions best, although the magnitude of the onset date anomaly was underestimated.

KEYWORDS
CORDEX, GCM, HighResMIP, Indonesia, monsoon, RCM, Southeast Asia

1 | INTRODUCTION

Global climate models (GCMs) are the primary tools used to assess the impact of climate change. The reliability of GCMs in projecting climate change depends on the skill of the models in simulating the present-day climate (Raäisaänen, 2007). The representation of the hydrologic cycle in GCMs is still limited, although there have been improvements made on physical, biological and chemical processes (Ul Hasson *et al*., 2016). The spatial resolution of the models is one of the limitations that leads to a poor representation of the hydrologic cycle in GCMs as many of the processes contributing to the hydrologic cycle need to be resolved through parameterization schemes, such as convection. With this limitation, the assessment of future climate change impacts over Southeast Asia (SEA) is challenging since this region has unique physio-geographical characteristics (Ul Hasson *et al*., 2016).

Earlier research used rainfall gauges and gridded sea surface temperature (SST) data for the reproduction of the three observed dominant rainfall patterns in the Indonesian region (Aldrian and Susanto, 2003). In a follow-up of that study, the GCM results were downscaled using a regional climate model (RCM) aiming to test the hypothesis that the poor results were related to inadequate representation of the rainfall characteristics and a topography that was too coarse (Aldrian *et al*., 2004). The use of the RCM embedded in the global model clearly improved rainfall due to the more realistic topography. Changing the resolution of the GCM from 1.125° to 0.5° resulted in a dramatic improvement in rainfall over most of the Indonesian archipelago as well. In addition, the authors concluded that a prerequisite to realistic simulations of precipitation patterns is to account for the SST, which is the major factor determining the quality of the simulations. The region with the most realistic SST values had the smallest bias. Motivated by these results, follow-up research was conducted using long-term high-resolution (HR) coupled climate model simulations (Aldrian *et al*., 2005). The coupling produced a more realistic representation of SST and a lower overestimation of rainfall over the sea. Compared to the previous research that used the uncoupled model, the HR coupled model has accurately simulated rainfall over the region.

The ability of the climate model to simulate El Niño-southern oscillation (ENSO) circulation improves as the spatial resolution increases (Shaffrey *et al*., 2009; Masson *et al*., 2012). In addition, the modelled Atlantic inter-tropical convergence zone (ITCZ) (Doi *et al*., 2012) behaves more realistically. Further improvements are expected in the latest generation of GCMs from the HR model intercomparison project (HighResMIP; Haarsma *et al*., 2016). These models are run at spatial resolutions similar to that of RCMs. For Europe, the HR GCM and the RCM show similar strengths and weaknesses in terms of daily precipitation distribution (Demory *et al*., 2020). For SEA however, the added value of the HighResMIP approach in comparison to the downscaling approach of RCMs needs to be investigated, especially for the aspect of the monsoon characteristic.

As global warming affects both the mean precipitation and the precipitation variability (Seager *et al*., 2012), a higher frequency of dry spells may be possible (Lintner *et al*., 2012). This condition may impact the monsoon rains which are very important for agriculture in SEA (Marjuki *et al*., 2016). The onset of the monsoon season is essential for farmers in SEA. Observations have shown a negative correlation between paddy rice yield and a delayed onset for some Southeast Asian countries (Marjuki *et al*., 2016). A delayed onset can prevent a farmer from having three annual crops, which is projected in some climate scenarios (Naylor *et al*., 2002).

The monsoon characteristics relate not only to local conditions but also to large-scale structures like the ITCZ (Nieuwolt *et al*., 1977; Aldrian and Susanto, 2003). This means that a global HR model might have an advantage over a low-resolution (LR) GCM with an embedded RCM as the former is expected to simulated large-scale structures more realistically. The HR models of HighResMIP may show similar levels of detail and realism in precipitation over complex topography as the RCMs, combined with the benefit of a more correct large-scale ITCZ.

This study aims to assess model performance in simulating the monsoon characteristics for SEA. We also investigate the effect of ENSO on the monsoon. A robust

climate change impact assessment in the region must be based on climate models, which have a good representation of the onset of the monsoon rainfall. Here, we will compare the HighResMIP against observations and the downscaled result of the Coupled Model Intercomparison Project phase 5 (CMIP5) from the coordinated downscaling experiment (CORDEX) SEA simulations (Giorgi *et al*., 2012; Yang, 2012; Juneng *et al*., 2016; Ngo-Duc *et al*., 2017; Supari *et al*., 2020; Tangang *et al*., 2020), focusing specifically on monsoon characteristics. We will also compare the HR configuration of the HighResMIP models against their LR equivalents.

2 | MATERIALS AND METHODS

2.1 | Description of the study area

The SEA domain that we analyse covers the area between 12.5°S–24.5°N and 92.5°E–142.5°E and includes the northern part of Myanmar, Laos, Vietnam, Thailand, Cambodia, Malaysia and Indonesia. The wet season in the SEA is part of the Australia-Asia monsoon system. The system is situated between the centre of the Asian summer monsoon and Australian summer monsoon and spans the East Asia region, including the northern part of Australia (Wang, 2006).

The ITCZ crosses the equatorial region (between 10° and −5° latitude) twice a year. Most of the area in this region has two rainy seasons, the first during boreal spring and the second during boreal autumn with a higher peak in the second season (Aldrian and Susanto, 2003). The temporal development of the monsoon over the region has been described in earlier publications (Hamada *et al*., 2002; Aldrian and Susanto, 2003; Moron *et al*., 2009).

2.2 | DATA

2.2.1 | Observation

In the SEA, the density of gauges and the long-term availability of rainfall time series are limited, which makes the development of a dataset for daily precipitation amounts based on in-situ measurements challenging (Van den Besselaar *et al*., 2017; Singh and Xiaosheng, 2019). To account for the uncertainty in observed rainfall, a total of three gridded daily observational datasets are used in this study. The first dataset is the Southeast Asia Observation (SA-OBS) (Van den Besselaar *et al*., 2017). SA-OBS is a daily HR land-only observational gridded dataset for precipitation and minimum, mean and maximum temperatures covering the SEA region. This dataset is used in its 0.5° by 0.5° regular latitude-longitude grid for the period from 1981 to 2016. The observational data on which SA-OBS is based is collected by the Southeast Asian Climate Assessment & Dataset (SACA&D), a cooperation between Indonesia's meteorological service and other meteorological services in the region (Van den Besselaar *et al*., 2015). As a result of this cooperation, 1,394 precipitation stations, 365 stations with minimum and maximum temperature, and 274 stations with daily mean temperature have been selected.

The second dataset is the Asian Precipitation Highly Resolved Observational Data Integration towards Evaluation of Water Resources (APHRODITE; Yatagai *et al*., 2012). The APHRODITE (APHRO) daily precipitation data were created by collecting and analysing rain gauge observation data across Asia. The interpolation algorithm for the latest version of APHRO is similar to that presented by Yatagai *et al*. (2009) with improvements in weighting function to consider the effect of mountain ranges by giving high weight to gauges on slopes inclined to the target location and low weight to gauges on the leeward side behind a mountain ridge. The dataset is used to evaluate the model skill in simulating daily precipitation, including the precipitation extremes.

The third dataset is the Climate Hazards group Infrared Precipitation with Stations v2.0 (CHIRPS; Funk *et al*., 2015). The CHIRPS product provides daily precipitation data at a spatial resolution of 0.05° for the quasi-global coverage of 50°N–50°S from 1981 to the present. The CHIRPS was created using data from rain gauge stations collected from food and agriculture organization and global historical climate network, the Cold Cloud Duration information based on thermal infrared data archived from climate prediction center and NOAA National Climate Data Center (NCDC), the Version 7 TRMM 3B42 data, the Version 2 atmospheric model rainfall field from the NOAA Climate Forecast System, and rain gauge station data from multiple sources.

There is good agreement between the observation datasets on the mean onset of the rainy season in SEA (Figure 1). Figure 1d shows that the general movement of the onset of the rainy season is in line with the movement of the ITCZ. The zonal mean plot shows that the onset date moves to later dates for latitudes closer to the equator, but local detail is lost in this aggregated view. The Maritime Continent of SEA has a complex seasonal cycle of rainfall, which means that some areas end up having a local characteristic that is different from the movement of the ITCZ (Aldrian and Susanto, 2003).

Between the three gridded rainfall datasets, the SA-OBS dataset was specifically generated for the SEA using gauged rainfall stations. The dataset has been considered more accurate and reliable as compared to other datasets (Van den Besselaar *et al*., 2017; Ge *et al*., 2019), but the

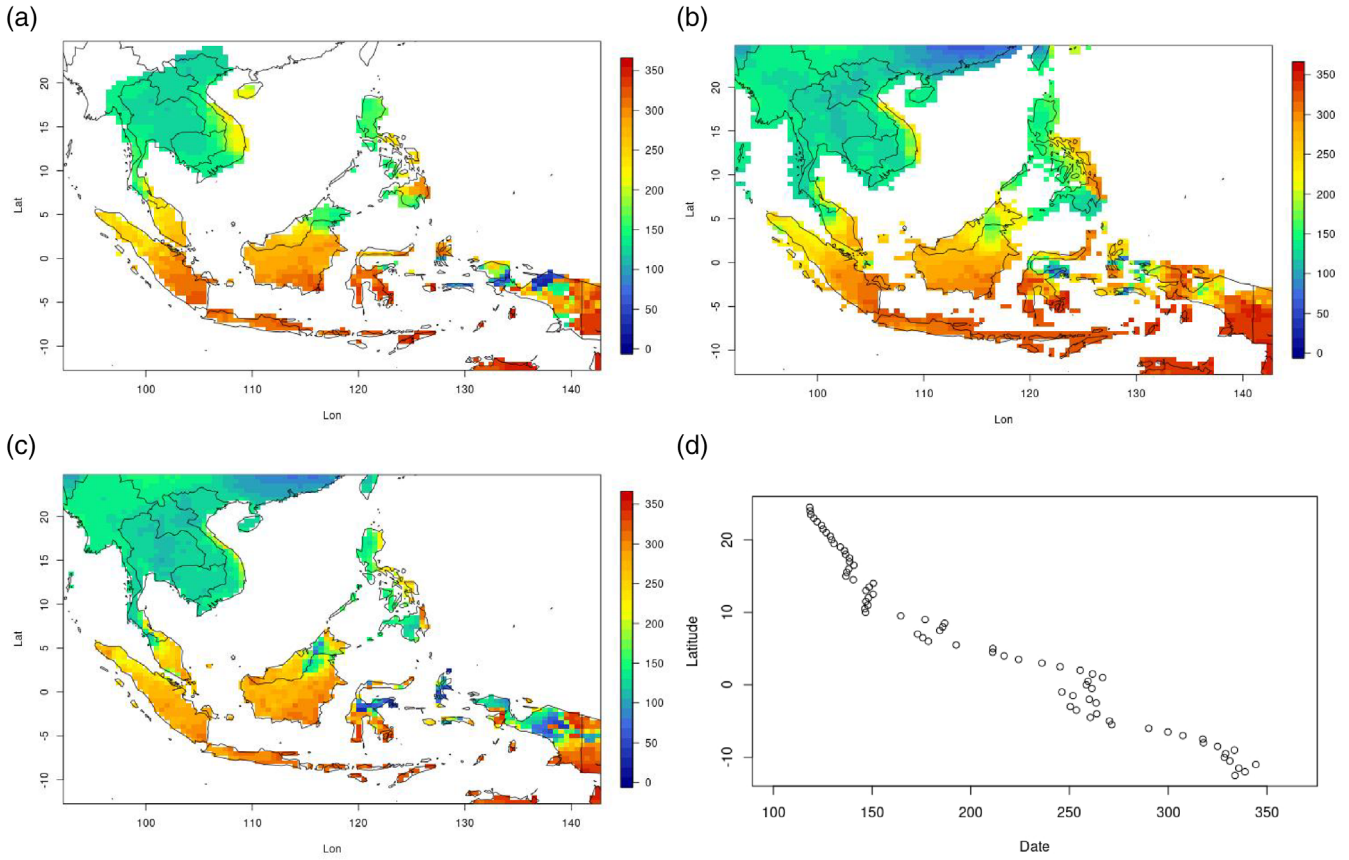

FIGURE 1 Map (SA-OBS (a), APHRO (b) and CHIRPS (c)) and zonal mean (d) of the mean onset of the rainy season in SEA. The mean and zonal mean onset is calculated from observation datasets (SA-OBS, APHRO and CHIRPS) for the period 1981–2005 [Colour figure can be viewed at wileyonlinelibrary.com]

restrictions on the search radius in the interpolation method have as a consequence that in areas that are too data-sparse, no interpolated values are calculated. The other two datasets use other approaches or more permissive interpolations and cover the complete land area of SEA.

2.2.2 | Model data

In this study, two classes of model experiment results are compared to the observation. The first model output is the downscaled version of CMIP5. We use six downscaled CMIP5 model datasets. The data of CNRM, CSIRO, EC-Earth and MPI were downscaled using RegCM4 (Giorgi *et al.*, 2012) by CORDEX SEA (Ngo-Duc *et al.*, 2017; Supari *et al.*, 2020; Tangang *et al.*, 2020), whereas HadGEM was downscaled using regional Weather Research and Forecasting (WRF3.5) (Skamarock *et al.*, 2008) by the Asia-Pacific Economic Cooperation Climate Centre (APCC) (Yang, 2012). The RCMs were run over the historical period 1971–2005. We will refer to the 6 model dataset as CORDEX.

The second model experiment output is from the HighResMIP experiment. The HighResMIP data are available from the H2020-funded Primavera project. In this project, GCMs were run at a spatial resolution comparable to that of the CORDEX models. We use two experiments of HighResMIP in this study. The first HighResMIP experiment is the coupled historic runs for the period 1950–2014 (Hist-1950). Fixed historical atmosphere and SST forcing from 1950 was applied for the spin-up period, after which a historically-evolving forcing was imposed (Haarsma *et al.*, 2016). Six HR models from the Hist-1950 experiment were used including EC-Earth (Haarsma *et al.*, 2020), MPI (Müller *et al.*, 2018), HadGEM (Roberts *et al.*, 2019), CMCC (Cherchi *et al.*, 2019), CNRM (Voldoire *et al.*, 2019), and ECMWF (Roberts *et al.*, 2018). EC-Earth and ECMWF are available in two and four members, respectively. For other models, there is only one member available. Later in this study, the HR of Hist-1950 model experiment will be called HR-Hist-1950.

The second HighResMIP experiment is the historically forced atmosphere run for the period 1950–2014 (HighresSST). This experiment used the daily 1/4° HadISST2-based dataset as the SST and sea-ice forcing.

With the extended period and HR simulation, it is expected that this experiment will improve upon the realism of the ENSO teleconnection (Sterl *et al*., 2007). This study used HR and LR simulation from the HighresSST. The same six models from the Hist-1950 experiment were used for the HighresSST experiment. There is only one member available for the CMCC, CNRM and MPI, both for the HR and LR simulations. For EC-Earth, there are three members available both for the HR and LR simulations. For ECMWF, there are four and eight members available for the HR and LR simulations, respectively. For the HadGEM, three and five members are available for the HR and LR simulations, respectively. More detailed information on the HighResMIP experiment can be found in Haarsma *et al*. (2016). Considering CORDEX, four models are available in HighResMIP (CNRM, EC-Earth, HadGEM and MPI). The remaining two models are different (CSIRO and GFDL for CORDEX, also CMCC and ECMWF for HighResMIP), which is due to the limitation of the data that are available from the CORDEX-SEA and Primavera project. In addition to the CORDEX and HighResMIP datasets, the EC-Earth GCM from CMIP5 with an ensemble of four members was used to support the conclusions, each member representing a perturbation in realization.

For the analysis, we interpolate the model and observation datasets to the same grid resolution; the reference resolution is 0.5°. We used bilinear interpolation to interpolate a dataset with higher resolution than the reference. Also, we used nearest-neighbour interpolation to interpolate datasets with a lower resolution than the reference. Information about the model configurations is shown in Table 1.

2.3 | Methods

2.3.1 | Season onset definition

There are various ways to quantify the onset (and cessation) of the rainy season. In the model context, it is possible to calculate sophisticated indices (including for example, wind direction at higher elevations and reference of evapotranspiration) (Zeng and Lu, 2004; Diong *et al*., 2019; Wati *et al*., 2019) but the observational datasets lack parameters other than temperature and precipitation, which limits us to applying the most straightforward indices. Marjuki *et al*. (2016) compared a few of these simple indices and despite a quantitative lack of similarity between the indices (although they are strongly correlated), we used the onset definition developed by Liebmann *et al*. (2007) as this index is applicable to the variations of climate in SEA.

We used the Liebmann *et al*. (2007) definition to define the rainy season onset and retreat. This definition is based on time series of daily sums of precipitation, which makes it specific for each location. It is calculated by

$$A(\text{day}) = \sum_{n=1}^{\text{day}} R(n) - \overline{R} \tag{1}$$

where A is the 'anomalous accumulation', $R(n)$ is the daily precipitation and $\overline{R}$ is the yearly average daily precipitation. The onset (retreat) of the wet season is defined as the absolute minimum (maximum) of A, indicating that the daily precipitation total from that date onwards is larger (lower) than the average daily precipitation.

The approach followed by Liebmann *et al*. (2007) used average daily precipitation calculated over a climatological mean period, but in this study, we use precipitation amounts calculated annually. This approach allows the onset and the retreat dates to be calculated for every year, including excessively wet or dry years, which may not be the case when using the climatological values (Marjuki *et al*., 2016).

In this paper, the accumulation period starts on January 1st for every year. This condition makes the onset date that is calculated for areas with two rainy seasons in the equatorial region represents the second rainy season. The index is calculated when at least 350 days of the year have non-missing data. This condition is only relevant for SA-OBS and APHRO as they have some missing data. Furthermore, we calculate the onset for all available members of the ensemble and show the mean of the ensemble.

2.3.2 | Validation methods

We use the Taylor diagram to compare the climatological mean values of the onset dates of the climate models. The *x*-axis and *y*-axis show the normalized standard deviation (*SD*). We use the observation *SD* for the normalization. Therefore, the closer the model normalized *SD* is to 1, the closer the model *SD* is to the observation *SD*. The curve axis shows the correlation between the spatial distribution of the model and the observation. The correlation calculation was made over the complete land area. The number of the grid box is the sample range for the correlation calculation.

We also calculate bias and normalized root mean square error (NRMSE) based on the climatological mean and median. In the calculation, the climatological mean and median were calculated for each grid cell. Furthermore, the indicators were calculated for each model,

TABLE 1 Description of the models, showing for each model in the first column, its horizontal resolution of the global model as used in CMIP5 and the resolution of the regional model from CORDEX for which it provided lateral boundaries

Model	CMIP5	CORDEX	HR Hist-1950	HR HighresSST	LR HighresSST
CMCC-CM2			25 km native atmosphere regular grid 1 member	25 km native atmosphere regular grid 1 member	1° × 1° native atmosphere regular grid 1 member
CNRM5 (CORDEX) CNRM-CM6-1 (HighResMIP)		25 km resolution 1 member	50 km regridded from T359l 1 member	50 km regridded from T359l 1 member	250 km regridded from T127l 1 member
CSIROMk36		25 km resolution 1 member			
EC-Earth (CORDEX) EC-Earth3 (HighResMIP)	Grid T159L62 4 members (realization)	25 km resolution 1 member	50 km grid T511 2 members (Physics version)	50 km grid T511 3 members (Physics version)	100 km grid T255 3 members (Physics version)
ECMWF-IFS			0.5° × 0.5° regridded from Tco399 6 members (Realization)	0.5° × 0.5° regridded from Tco399 4 members (Realization)	1° × 1° regridded from Tco199 8 members (Realization)
GFDL		25 km resolution 1 member			
HadGEM2-AO (CORDEX) HadGEM3-GC31 (HighResMIP)		25 km resolution 1 member	50 km grid N512 1 member	50 km grid N512 3 members (Initialization)	250 km grid N96 5 members (Initialization)
MPI-ESM (CORDEX) MPI-ESM1-2 (HighResMIP)		25 km resolution 1 member	50 km spectral T255 1 member	50 km spectral T255 1 member	100 km spectral T127 1 member

Note: The fourth, fifth and sixth columns specify the global resolution and the number of available members of the ensemble for ocean–atmosphere coupled high resolution (HR) simulations using initial conditions from 1950, historically forced high resolution atmosphere-only simulations and their low resolution (LR) equivalents, respectively.

using the number of grid cells as the sample range. The climatological bias (mean difference) and median difference are used to quantify the similarity in the climatological condition between models and observations. The NRMSEs are used to measure the deviation between simulated and observed values (Randall *et al*., 2007). The NRMSE value is expressed as a percentage (%), and it uses the standard deviation of observation data to normalize the RMSE.

The three observation datasets (SA-OBS, APHRO and CHIRPS) were combined into one pooled observation series as the reference. Combining these three datasets in this way gives us a straightforward way of accounting for the uncertainty of the observational estimates. A model simulation is compared to the pooled observations so that the comparison metric, like correlation, is based on a comparison against all three observational datasets. Furthermore, for the models run in ensemble mode, the ensemble-mean of the statistic indicator values is used.

In addition, we use the two-sample Kolmogorov–Smirnov test (K–S index) as an evaluation metric (Wilks, 2011). The indicator evaluates the difference in cumulative distributions between the observations and the model simulations. A smaller Kolmogorov–Smirnov statistic (K–S index) value indicates a better representation of model simulation for the data distribution. The K–S index was calculated for each grid box and used every year in the time range to build the cumulative distribution. For the cumulative distributions, the model members need not be averaged and are pooled into the sample.

3 | RESULTS

3.1 | Model performance on rainy season simulation

3.1.1 | Onset of rainy season

In general, we found a similar pattern of the mean rainy season onset in the models (Figure S1) as compared to the observations (Figure 1). The onset progresses from

May for the northern part of the region to the end of the year for the southern part of the region. Some models also reproduce the contrasting onset patterns of some areas in Sulawesi, Maluku and Papua (−5°–2° latitude and 120°–135° longitude) that have a different annual rainfall pattern than other areas at the same latitude (Aldrian and Susanto, 2003).

Tailor diagram (Figure 2) shows that in general, the *SD* values of the CORDEX models are closer to the observations as compared to the HighResSST and Hist-1950 models. In addition, the spatial correlations of the climatological onset of the rainy season are between 0.6 and 0.8 for most models. The model simulations are compared against the reference based on the pooled observational datasets. Hence, the simulations describe the movement of the monsoon well. The HighResMIP simulations show (considerably) higher spatial correlation with the observations as compared to the CORDEX. Among the HighResMIP simulation, we find a similar spatial correlation between the atmospheric model with the prescribed SST experiment (HighResSST) and the coupled model experiment (Hist-1950). This is also the case between HR and LR of HighResSST. Overall, there is no significant improvement of CORDEX results compared to the single CMIP5 model. Also, there is no significant improvement of HR HighResSST compared to LR HighResSST. However, in some models, like the MPI model, the spatial correlation of HighResSST is higher than Hist-1950. For the CNRM, the LR HighResSST is higher than the HR HighResSST.

Figure 3 presents the model bias of the climatological onset of the rainy season. We find a similar pattern of bias distribution between the three model experiments. There is more bias for the region around 5°S–10°N, the models tend to have an early-onset compared to the observations except for the area around 115–140°W where the models tend to have a late-onset compared to the observations.

Figure 4 presents a boxplot of the climatological bias and median difference of the models in simulating the onset of the rainy season. This figure shows data aggregated over the land area of the domain. The simulated monsoon onset in the CORDEX experiment is slightly closer to the observation as compared to a single CMIP5 model. However, a better simulation is shown with the HighResMIP experiments as indicated by the bias and median difference. Most HighResMIP models have biases less than ±25 days for the majority of the grid cells, which is much less than what is simulated in CORDEX. In terms of the HighResMIP experiments, the percentage of grid cells with ±25 days bias amount to 58–75% for LR HighResSST, 56–74% for HR HighResSST, and 57–73%. However, for CORDEX, this value amounts to 50–58% and 55% for a single CMIP5 model (Figure S2). The enhanced realism is confirmed by the NRMSE value, the average for HighResMIP models is 63% for LR HighresSST, 64% for HR HighresSST and 69% for HR Hist-1950. The average NRMSE for CORDEX models is 80%, which is slightly lower than the single CMIP5 model with an NRMSE of 83% (Figure S3).

The two-sample Kolmogorov–Smirnov test (K–S index) (Wilks, 2011) evaluates the difference in cumulative distributions between the observations and the model simulations. A small indicator value represents a close similarity between observations and model results. The K–S index for the onset of the rainy season confirms that the HighResMIP models represent the onset date distribution substantially better than CORDEX models. Meanwhile, we find a similar performance between CORDEX models and a single CMIP5 model (Figure 5).

Among the CORDEX models, the ones with lateral boundary conditions from the global EC-Earth simulation show high biases (Figure 4), NRMSE (Figure S3) and K–S index (Figure 5) of the onset of the rainy season. On average, CNRM, CSIRO and HadGEM tend to delay the onset, whereas the downscaled EC-Earth, GFDL and MPI tend to advance the onset. Compared to other CORDEX models, CNRM shows the smallest biases and MPI shows the lowest NRMSE (Figure S3) and K–S index (Figure 5).

Among the HighResMIP experiments, HighResSST shows slightly smaller bias, K–S index and NRMSE compared to the Hist-1950. Furthermore, comparisons between HR and LR of HighresSST based on the climatological mean and median biases, the NRMSE, and the K–S index, show similar skill in simulating the onset for both resolutions.

In the HighResMIP, ECMWF shows the smallest biases and also the lowest NRMSE and K–S index. For the LR HighResSST experiment, the CNRM, HadGEM and MPI tend to overestimate (late) the onset date, while EC-Earth, CMCC and ECMWF tend to underestimate (early) the onset date. Whereas for the HR HighResSST experiment, except for the CNRM, most of the models tend to underestimate (early) the onset date. For the HR Hist-1950 experiment, the CNRM, HadGEM and MPI tend to overestimate (late) the onset date, while EC-Earth tends to underestimate (early) the onset date.

3.1.2 | Total precipitation

We now turn our attention to the simulation of the accumulated rainfall (total rainfall) over the monsoon season. The total rainfall of the rainy season is calculated based on the 6 months following the zonal mean onset of the wet season (Figure 1d) and is the cumulative value over these 6 months. A comparison of the three different

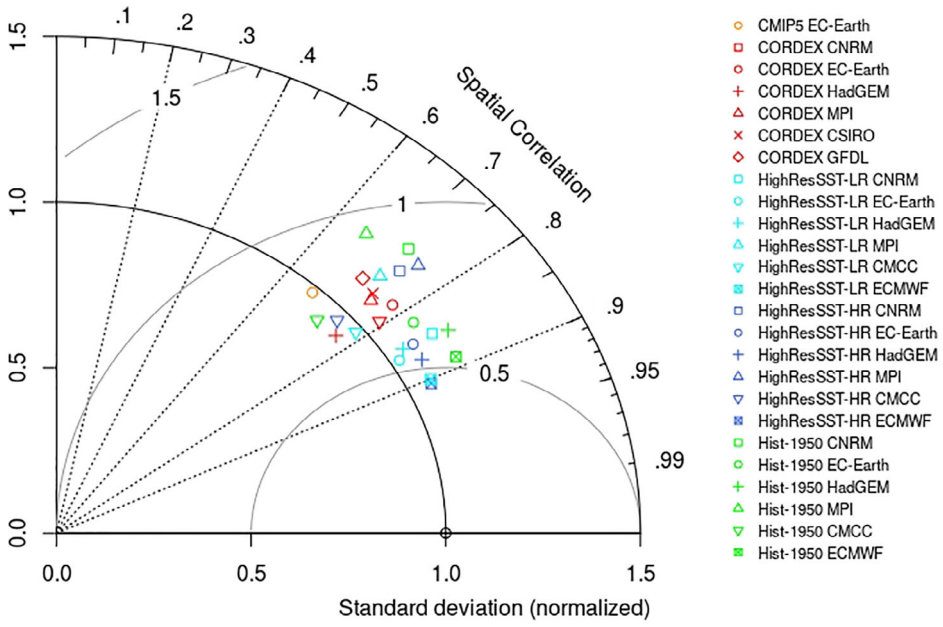

FIGURE 2 Taylor diagram of the onset of the rainy season. The *x*-axis (*y*-axis) shows the normalized *SD* of the onset date. The curve axis shows the spatial correlation [Colour figure can be viewed at wileyonlinelibrary.com]

climate model experiments in terms of the spatial correlation in total rainfall maps shows that the downscaling process in the CORDEX improves the spatial correlation of the total precipitation, although the similarity with observations is not as high as in the HighResMIP (Figure 6). The CORDEX models have spatial correlations with the observations below .2 except for CNRM. For the HighResMIP, most of the models have a spatial correlation with the observed precipitation pattern exceeding .2, except for CMCC and MPI. HadGEM (MPI) shows the highest (lowest) spatial correlation among the HighResMIP models. Overall, we find a low correlation between modelled and observed spatial distribution of the total precipitation of the rainy season in the region. In terms of the *SD* value, we find that the HighResMIP and a single CMIP5 model show *SD* values to be closer to observations as compared to the CORDEX models.

Figure 7 shows the bias and difference in the median between observed and modelled total precipitation, where the precipitation accumulates over the rainy season. This figure clearly shows that the CORDEX models deviate more from observations than the HighResMIP and the single CMIP5 model. Most of the HighResMIP models and the single CMIP5 model have a NRMSE smaller than 150% which is considerably smaller than the NRMSE of the CORDEX models which are above 300% (except for the CSIRO model which is relatively low at 250%; Figure S4).

The K–S index values of the HighResMIP models are significantly lower than that of the CORDEX models. This indicates a closer resemblance of the HighResMIP model output to observations in terms of the cumulative distribution of total precipitation (Figure S5).

It is an unexpected result that the downscaled CMIP5 CORDEX models perform badly in terms of the mean and median biases, NRMSE and K–S index for the total amount of precipitation during the rainy season. One of the reasons was explained by Juneng *et al.* (2016), who found that the MIT-Emanuel convective scheme (Emanuel and Živković-Rothman, 1999) that was used in the RegCM4 RCM had simulated large positive precipitation biases. This condition explains the high simulated rainfall variability found by Nguyen-Thi *et al.* (2021). As an impact, we found that the total precipitation for the rainy season was very high for the CORDEX models. Similar results were also found by Amsal *et al.* (2019), using the same configuration of RegCM4 RCM for CSIRO Mk3.6 over Indonesia. The total rainfall bias they found was ±500 mm/month.

Among the models in the HighResMIP experiment, we found a slight improvement of the HR HighResSST compared to the LR HighResSST in the spatial correlation. However, the same condition is not found in the biases, NRMSE and K–S index. Overall, we observe similar performance between HighResSST and Hist-1950 experiments and between HR and LR HighResSST. All models excluding MPI and CNRM tend to overestimate the total precipitation. Compared to other HighResMIP models, EC-Earth and CNRM show the smallest and the largest biases, respectively.

3.2 | ENSO composite analysis for the onset simulation

3.2.1 | Understanding the effect of ENSO on the seasonal rainfall and the onset of the rainy season

In this ENSO composite analysis, we select the El-Niño years (1982, 1987, 1991, 1997, 2002 and 2004) and the

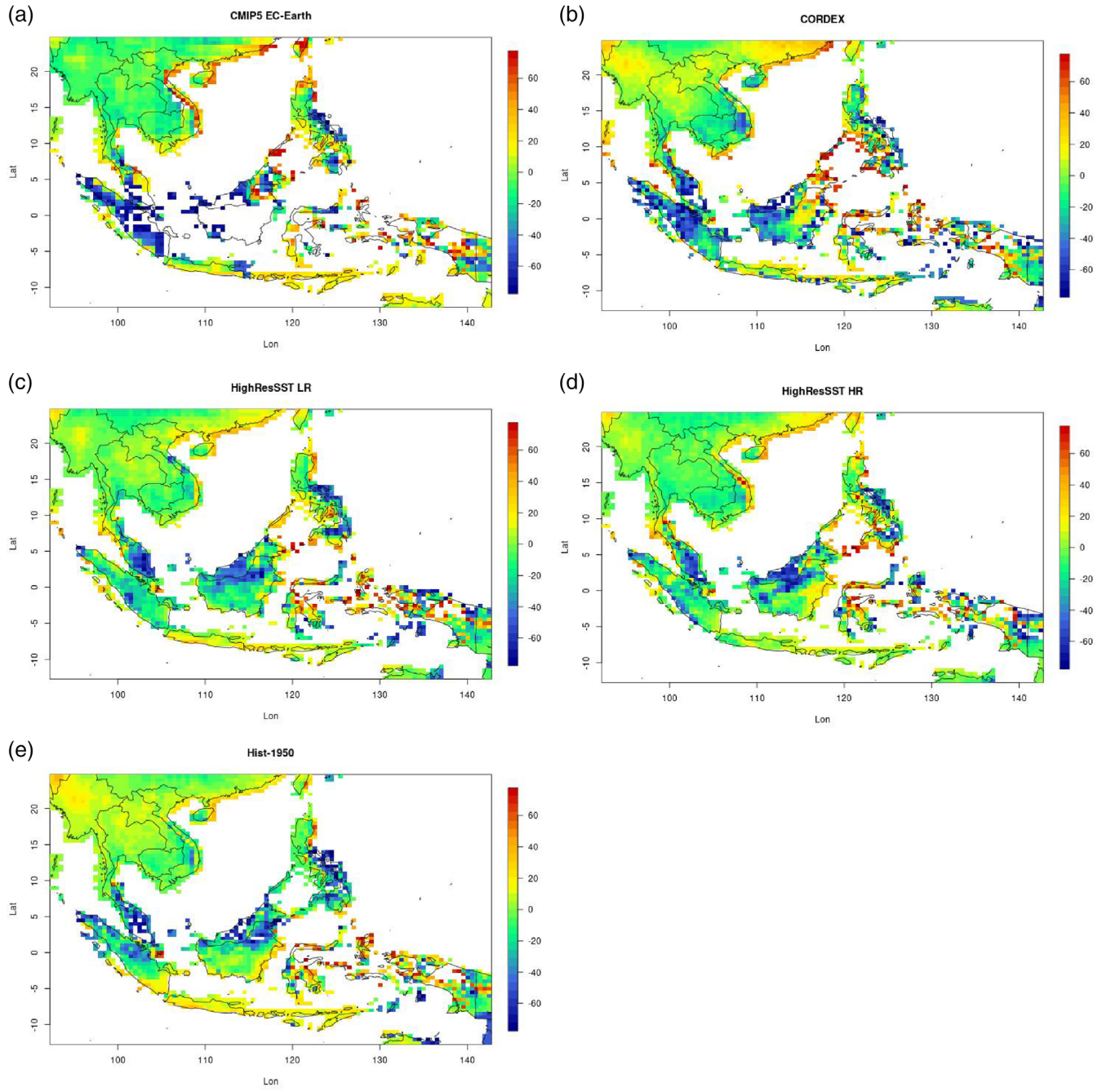

FIGURE 3 Map of difference between ensemble mean model experiment and observation on climatological onset of the rainy season in SEA. The model experiments are CMIP5 (a), CORDEX (b), LR HighresSST (c), HR HighresSST (d) and HR Hist-1950 [Colour figure can be viewed at wileyonlinelibrary.com]

La-Niña years (1988, 1995, 1998, 1999 and 2000) based on the Oceanic Niño Index (ONI) (NOAA, 2020). The El-Niño (La-Niña) years are selected using a threshold of eight consecutive months with negative (positive) ONI values.

Figure 8 shows the observed cumulative rainfall anomaly in the seasonal period of December–February (DJF), March–May (MAM), June–August (JJA) and September–November (SON) during the El-Niño years. During El-Niño years, the negative rainfall anomaly in DJF is located more over the Philippines and the northern part of Borneo and Sulawesi. A similar pattern is also found in MAM, but it is more spread out to the Malaysia Peninsula and the northwestern part of SEA. Meanwhile, during JJA and SON, the negative rainfall anomaly is located more over the southern part of SEA (below 5°N). In addition, for SON, the negative rainfall anomaly is spread more to the Philippines and Vietnam. We also

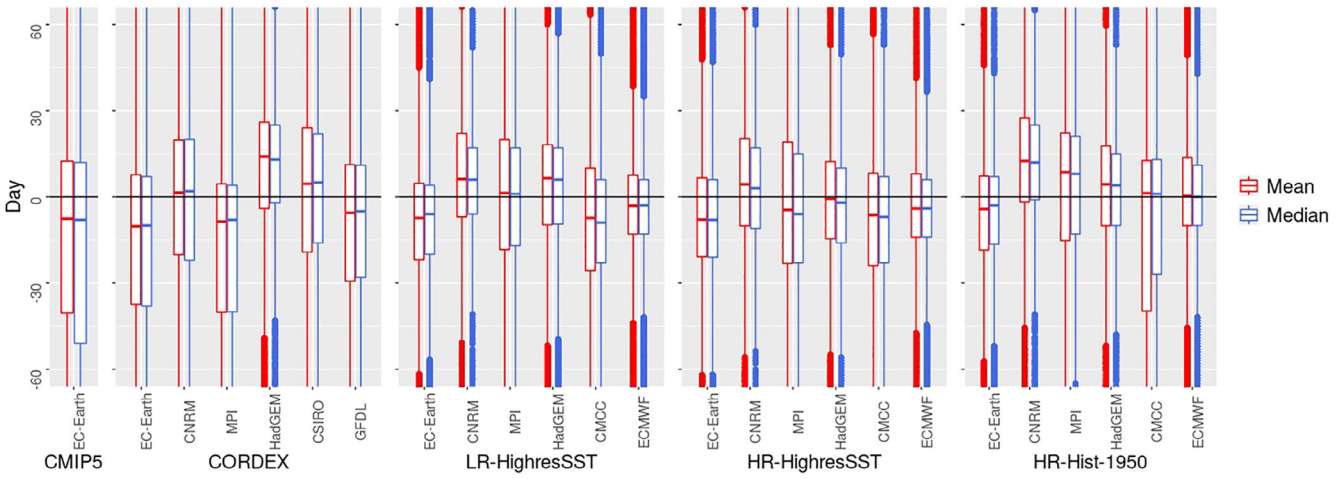

FIGURE 4 Mean and median model biases on the onset of the rainy season. Data are averaged over the region (land points only) and deviations are shown with respect to the observational dataset. The bolder dots at the ends of the whiskers are the outliers. The vertical axis is limited at approx. 60 days: most variations are in this time span [Colour figure can be viewed at wileyonlinelibrary.com]

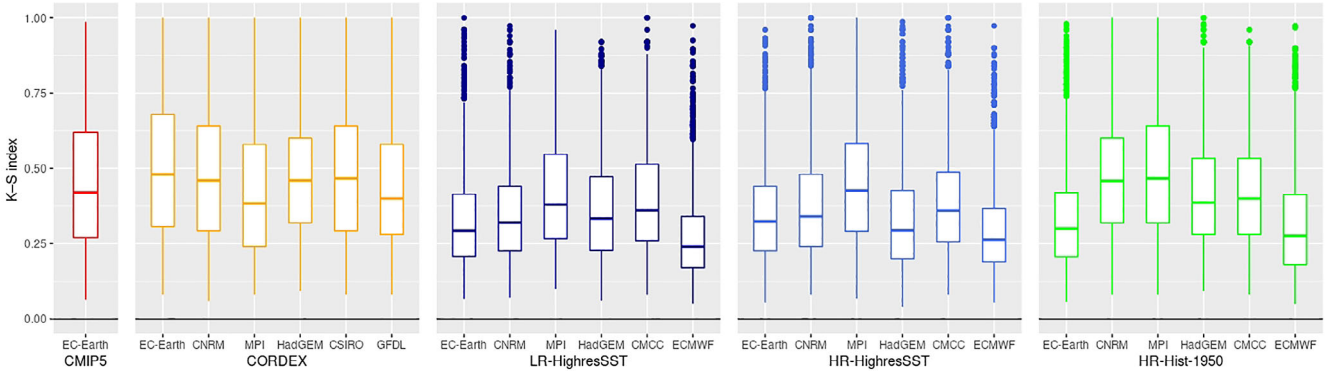

FIGURE 5 K–S index of the onset of the rainy season [Colour figure can be viewed at wileyonlinelibrary.com]

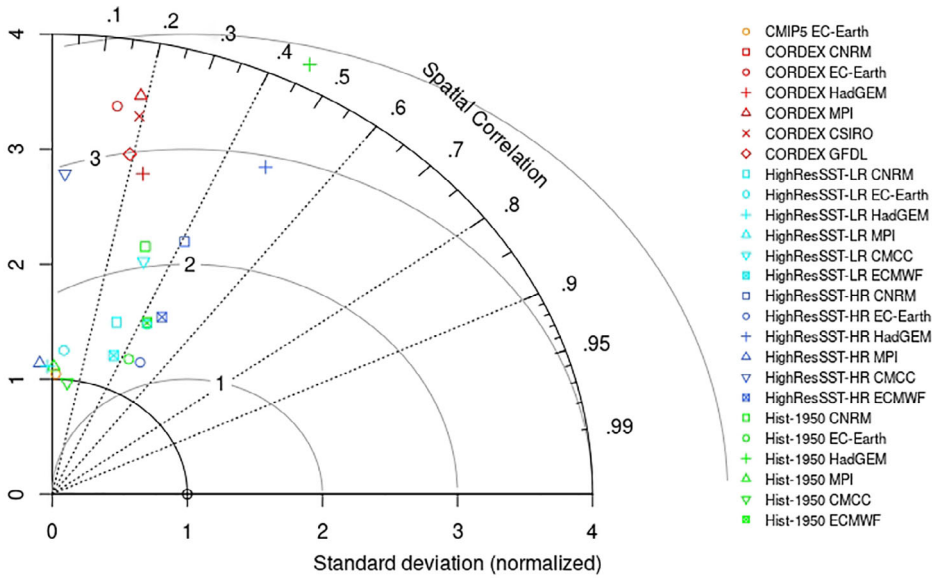

FIGURE 6 Taylor diagram of the total precipitation of the rainy season. The *x*-axis (*y*-axis) shows the normalized *SD* of the total precipitation of the rainy season. The curve axis shows the spatial correlation [Colour figure can be viewed at wileyonlinelibrary.com]

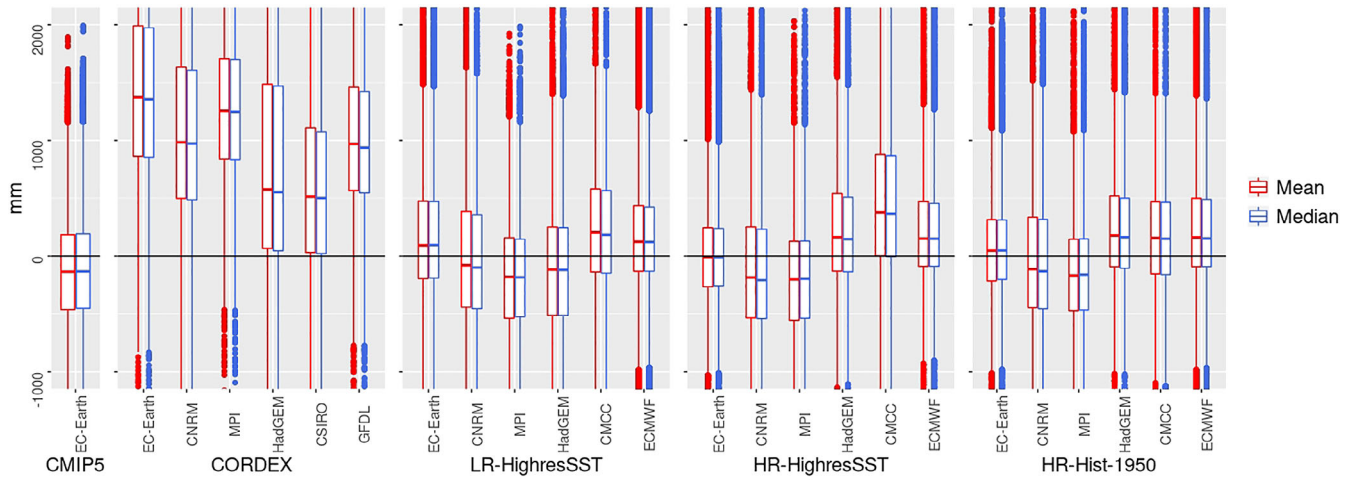

FIGURE 7 Mean and median models biases of the total precipitation of the rainy season. Data are averaged over the region (land points only) and deviations are shown with respect to the observational dataset. The bolder dots at the ends of the whiskers are the outliers. The vertical axis is limited at approx. −1,000 to 2,000 mm: most variations are in this time span [Colour figure can be viewed at wileyonlinelibrary.com]

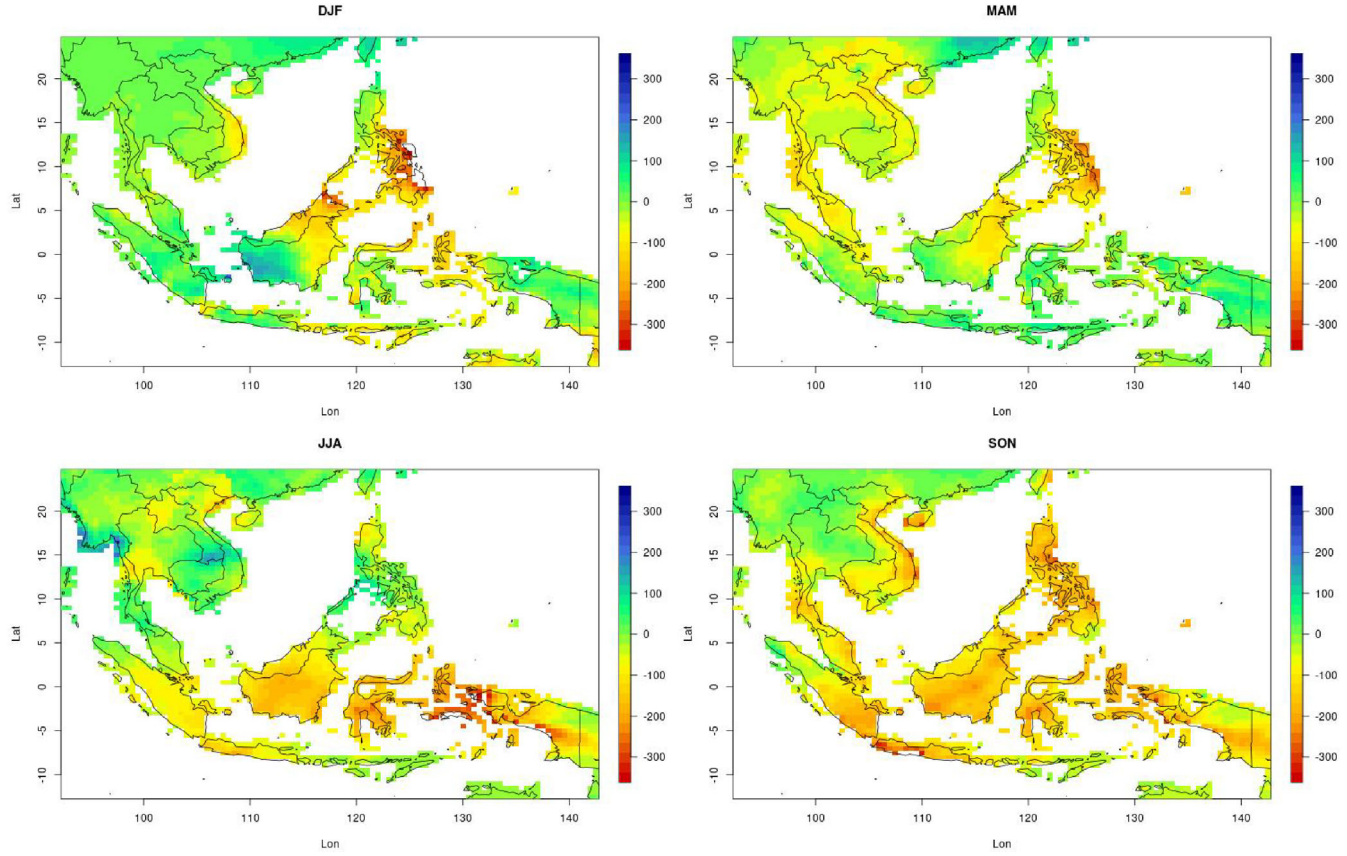

FIGURE 8 Map of rainfall anomaly during El-Niño year for seasonal period [Colour figure can be viewed at wileyonlinelibrary.com]

find that the positive rainfall anomaly during La-Niña years has a similar pattern to the negative anomaly during El-Niño years (Figure S6). These results are also found in an earlier study that analysed the correlation between precipitation and Nino3.4 index (Trouet and Van Oldenborgh, 2013).

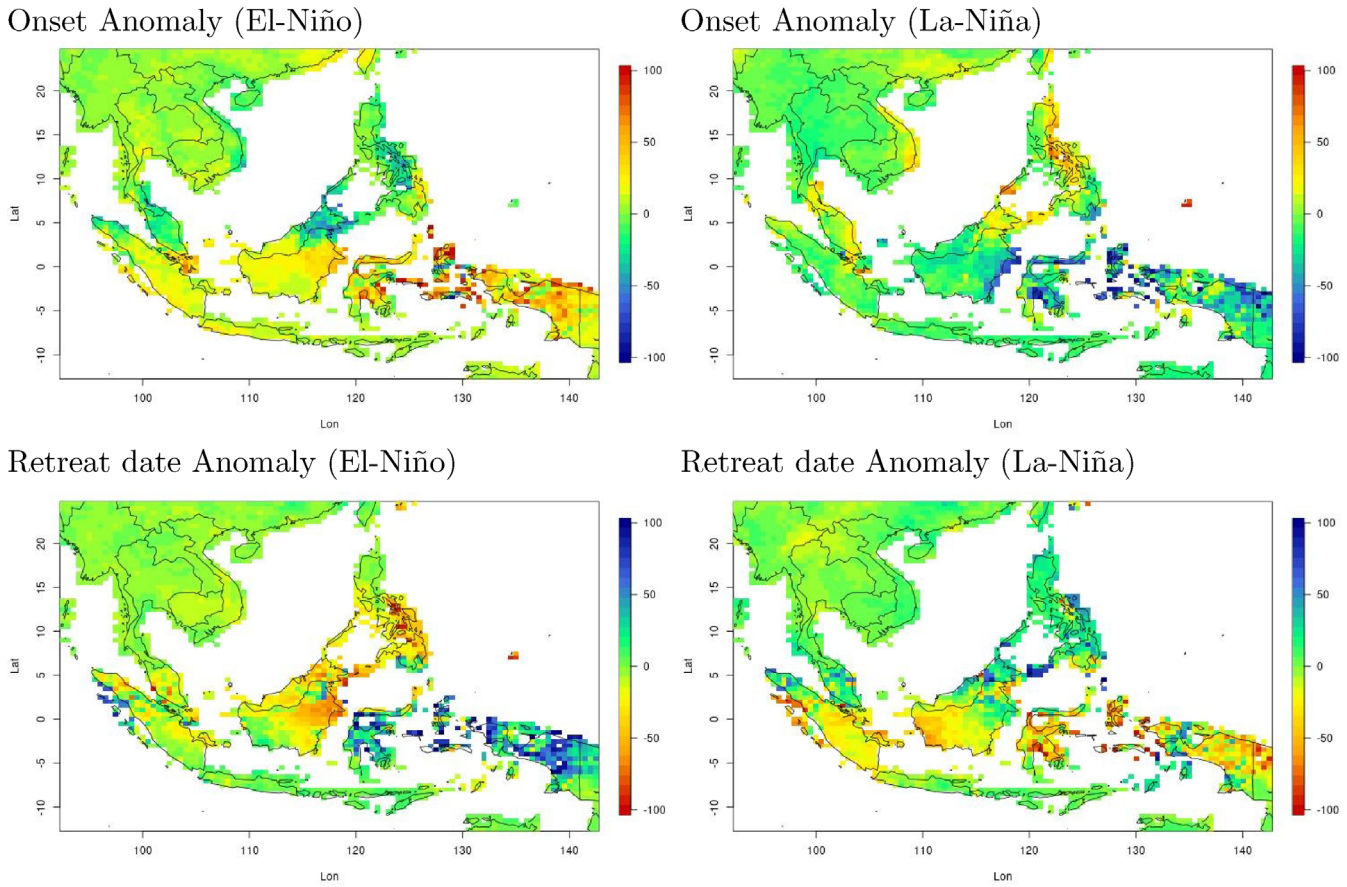

FIGURE 9 Map of the observed onset and the retreat dates of the anomaly during El-Niño and La-Niña years [Colour figure can be viewed at wileyonlinelibrary.com]

The dominant ocean surface currents during the DJF and MAM flow from the Pacific Ocean to the north of Papua and continues to flow northward to the Philippines before it flows southward to the Indonesian region through the South China Sea. Therefore, the effect of the ENSO condition of those two periods is stronger over the northern part of SEA (above the 0° latitude). Conversely, in JJA and SON, the dominant surface current flows directly to the Indonesian region from the Pacific Ocean through the northern part of Papua. As a result, the effect of the ENSO condition is stronger for the southern part of SEA (below 5°N; Wyrtki, 1961; Aldrian *et al*., 2007).

The effect of ENSO varies based on the time and place in SEA, and the impact of the effect of ENSO on the onset and the retreat dates of the rainy season also varies based on the place. The onset of the rainy season progression starts from the northern and continues to the southern part of the SEA during the period from May to the end of the year. In this period, the impact of ENSO is stronger for the southern part of SEA (below 5°N). As a result, we find more anomalies in the onset dates for this region. We find late (early) onset dates in El-Niño (La-Niña) years for the southern part of SEA. In contrast, there are tendencies of early (late) onset dates for the regions over the Philippines and the northern part of Borneo (Figure 9a).

Contrasting with the effect of the onset dates, we find an early (late) retreat date in El-Niño (La-Niña) years for the northern part of SEA (above 0° latitude). The retreat date progression in SEA generally starts in the northern part of SEA and moves to the southern part of SEA from September to May. The retreat date for the southern (below 5°N) part of SEA occurs in the period between January and May. In this period, the effect of ENSO is weak over this region. Therefore, we find a contrasting condition to the anomaly of the retreat date for the northern part in the anomaly of the retreat date for the southern part of SEA. Most of the southern part of SEA tends to have a late (early) retreat date in El-Niño (La-Niña) years (Figure 9b).

3.2.2 | Model performance of the effect of ENSO on the seasonal rainfall and the onset of the rainy season

In this section, we investigate the performance of the LR and HR models of the HighResSST experiment in

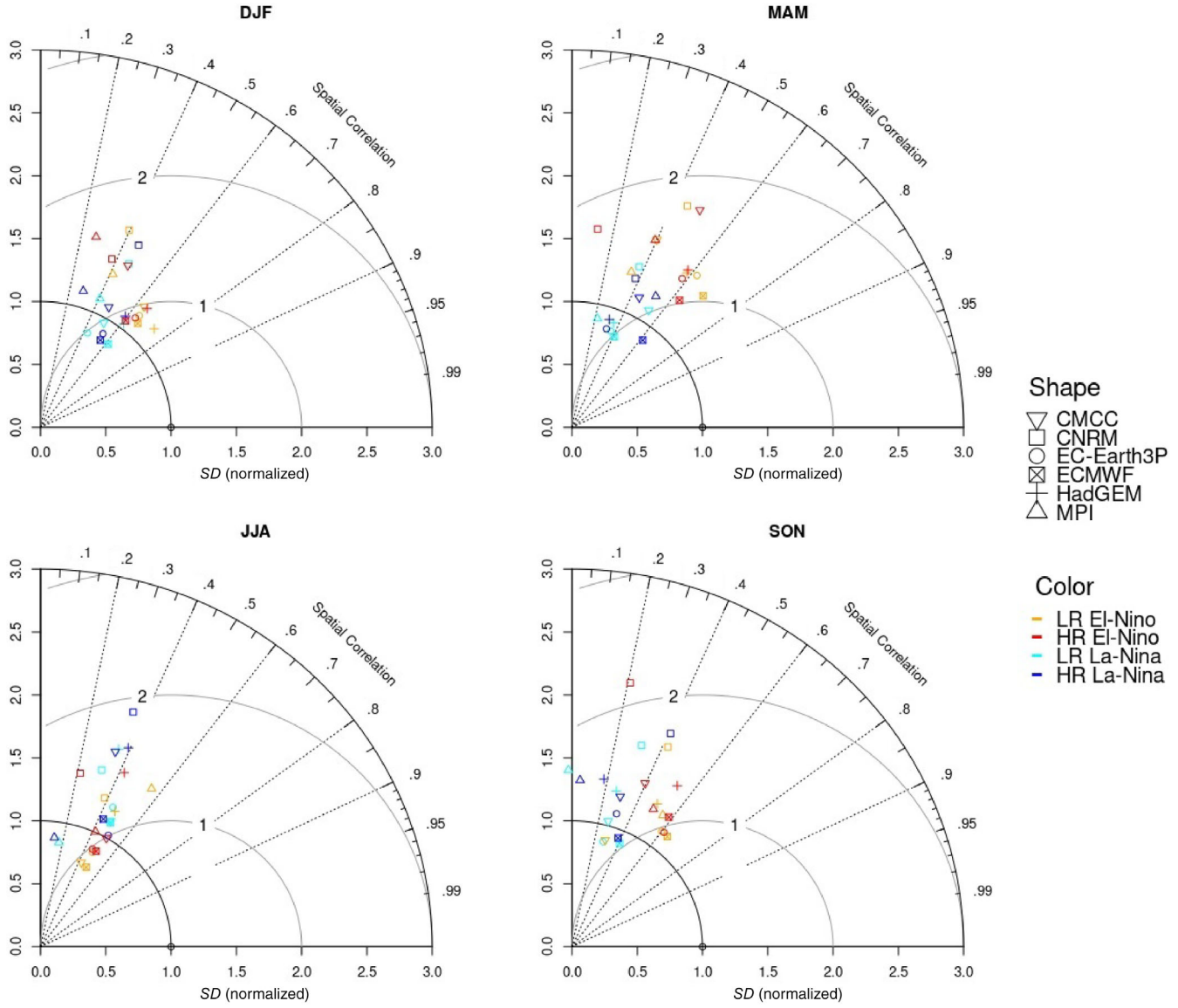

FIGURE 10 Taylor diagram of the rainfall anomaly during El Niño year for seasonal period. The *x*-axis (*y*-axis) shows the normalized standard deviation. The curve axis shows the spatial correlation [Colour figure can be viewed at wileyonlinelibrary.com]

simulating the onset of the anomaly in El-Niño and La-Niña years. The HighResSST experiment was forced by SST observation, which means that the model can be compared directly to the observations of the ENSO composite analysis.

Figure 10 shows the Taylor diagram of the rainfall anomaly for the seasonal periods during El-Niño and La-Niña years. Overall, based on the spatial correlation, the models simulate the rainfall anomaly better for El-Niño than for La-Niña. However, the *SD* of the models is closer to the observations when simulating the rainfall anomaly for La-Niña as opposed to El-Niño.

Furthermore, based on the spatial correlation values, we find that both resolutions (HR and LR) of HighResSST successfully capture most of the general pattern of the seasonal rainfall anomaly (Figures S7–S14). This is shown by the spatial correlation of the majority of the models that range between .4 and .6 (Figure 10). It shows that the correlation in DJF and MAM is higher than in JJA and SON. We find a similar performance between HR and LR HighResSST. This condition is confirmed by the rainfall anomaly (Figure S15) and the bias of the rainfall anomaly (Figure S16) of the models. Based on the spatial correlation, the rainfall anomaly and the bias of the rainfall anomaly of the models, we find that EC-Earth, ECMWF and HadGEM perform better as compared to the three other models.

Figure 11 shows the onset and the retreat date of the anomalies during El-Niño and La-Niña years. We found a late (early) onset during El-Niño (La-Niña) years in the

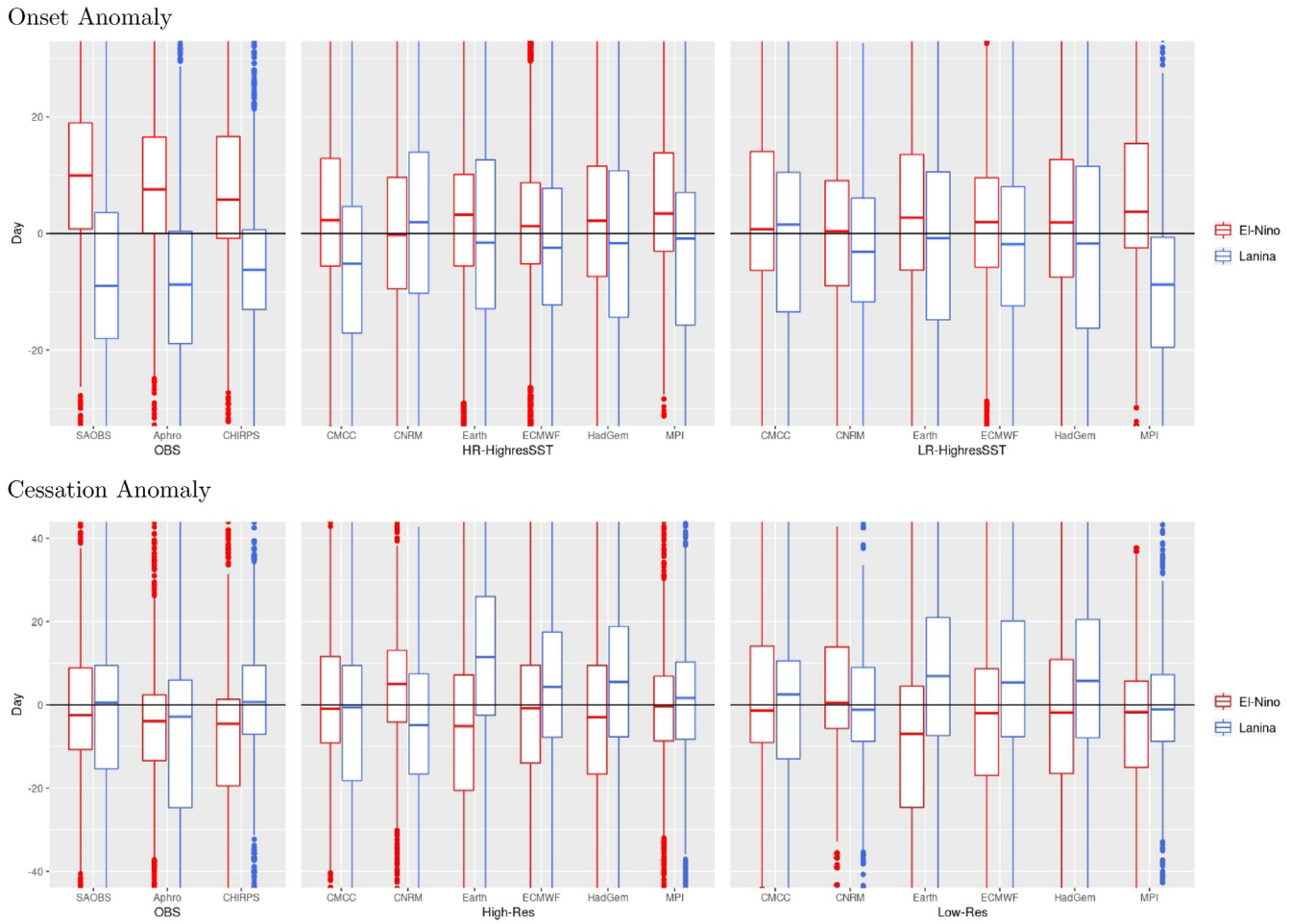

FIGURE 11 Boxplot of onset (top) and cessation (bottom) anomalies during El-Niño and La-Niña years [Colour figure can be viewed at wileyonlinelibrary.com]

observed anomalies for most of the grid cells over SEA. Except for CNRM, all models simulate the anomalies. However, the magnitude of the modelled anomaly is smaller than the observed anomaly. Overall, based on the anomalies of the onset and retreat dates, we found a similar performance between HR and LR HighResSST. This condition was confirmed by the spatial correlation and *SD* (Figure S21) as well as the bias of the anomalies (Figure S22) of the onset and the retreat dates. Looking at all the parametric measures, CMCC, EC-Earth, ECMWF and HadGEM perform better as compared to CNRM and MPI.

4 | DISCUSSION AND CONCLUSION

The performances of CORDEX and HighResMIP climate models on simulating the rainy season over the SEA region are investigated using the onset of the rainy season as the principal metric. The onset of the rainy season starts in May in the northern part of the region and moves to the southern part by the end of the year, except for some areas in Indonesia, which have a non-monsoonal rainfall pattern (Aldrian and Susanto, 2003). Wind, precipitation, and OLR data have been widely used for monsoon onset studies (Zeng and Lu, 2004; Diong *et al.*, 2019). In this study, we used a relatively simple monsoon onset definition developed by Liebmann *et al.* (2007), which uses only precipitation data. Despite the absence of wind that describes the circulation change on the monsoon development, the onset calculation from Liebmann *et al.* (2007) captures the movement of the monsoon onset in SEA.

We also assess the effect of ENSO on the monsoon date based on this definition. The impact of ENSO varies depending on time and place in SEA. As a result, we find late (early) onset dates for most of the Indonesian region (latitude <5°N) during the El-Niño (La-Niña) phases. This onset is then followed by a late (early) retreat date.

In contrast, we find early (late) onset dates followed by early (late) cessation for most of the area around the Philippines during El-Niño (La-Niña) phases. Meanwhile, the effect of ENSO on the onset and the retreat dates is weak over most areas in the northwestern part of SEA (Myanmar, Laos, Thailand, Cambodia).

We use three gridded daily observational datasets in this study. The SA-OBS is developed specifically for the SEA region using rain gauges from the national meteorological services in the region. SA-OBS has a higher density of data as compared to two other gridded datasets (APHRO and CHIRPS) especially over Indonesia, where most of the actual observations over Java and Sumatra are not available for scientific research. However, not all Southeast Asian countries in the domain of SA-OBS contributed to the dataset (Van den Besselaar *et al*., 2017). This creates some limitations with regards to covering some areas in the north of SEA. A restriction in the search radius of the interpolation method of SA-OBS means that the dataset has areas where no rainfall estimates can be given when data density is too low.

More spatial coverage was found in APHRO and CHIRPS datasets than in SA-OBS. Being developed from in-situ measurements and having a less restrictive interpolation method means that the APHRO dataset covers more area in SEA as compared to SA-OBS. However, the dataset has a lower station density in many parts of SEA as compared to SA-OBS (Van den Besselaar *et al*., 2017). Also, the CHIRPS dataset uses a recently produced satellite rainfall algorithm that combines climatology data, satellite precipitation estimates, and in-situ rain-gauge measurements to produce a HR precipitation product (Funk *et al*., 2015). The global coverage of this satellite data means that this dataset has better coverage compared to SA-OBS and APHRO. However, the number of rain gauges used to calibrate this dataset is lower than what is used in the other two observational datasets (Funk *et al*., 2015). Van den Besselaar *et al*. (2017) found stronger similarities between the gauge-based datasets than between the gauge-based datasets and the satellite-based datasets.

This study aims to compare the performance of HighResMIP against CORDEX in simulating the monsoon characteristics over the SEA region. The models from the HighResMIP suite were consistently closer to the observations than models from the CORDEX. Using bias, NRMSE and spatial correlation of the climatological mean and median value between model and observation as the key metrics in comparison, we find that the HighResMIP models simulate the onset date and the total precipitation of the rainy season over the region closer to the observations than the other model suits used in this study. Based on the Kolmogorov–Smirnov index, we also find that the HighResMIP models better represent the annual variation of the monsoon index. We found more general consistency in the HighResMIP model simulations compared to the CORDEX model simulations.

In terms of total precipitation analysis from the CORDEX models, we find that the uncertainty within a model and between models is substantial. Apparently, the downscaling process does not reduce uncertainty. However, for other analysis, we find that the CORDEX experiment has improved the model simulation of the monsoon.

This study is also interested in investigating the model performance of the effect of ENSO on the onset and the total precipitation of the rainy season. Here, we compare HR against LR of HighResSST models. In general, we find a similar performance of HR HighresSST and LR HighresSST on simulating the monsoon characteristic. Based on the El-Niño and La-Niña composite analysis, both HighresSST model experiments (HR and LR) simulated the anomaly of the onset and the total precipitation during different ENSO conditions with comparable skill. This is similar to an earlier publication that shows RCMs do indeed effectively reproduce variability during ENSO years (Aldrian *et al*., 2004). However, the models fail to completely follow the spatial distribution of the onset and retreat date anomalies of the observation. In addition, the magnitude of the onset anomaly of the model is still lower as compared to the observations.

Overall, we find no significant improvement of HR HighresSST as compared to LR HighresSST on the El-Niño and La-Niña composite analysis. This finding is different than previous study results where the LR model was unable to capture the growth of the coupled disturbance in the developing phase of ENSO, whereas the HR model does capture these disturbances (Gualdi *et al*., 2005). With this contradiction, we argue that the high skills in the HighresSST experiments relate to the prescribed SSTs rather than the more detailed atmospheric dynamics.

In conclusion, we find that the HighResMIP experiment has a better simulation as compared to the CORDEX experiment. As for the HighResMIP experiment, we find a similar performance of the HighResSST experiment compares to the Hist-1950 experiment. In the same vein, the HR performed the same as the LR.

There is a high demand for a HR dataset for climate and climate change analysis. We conclude that the HighResMIP experiment models in higher resolutions with better representations of the monsoon characteristics in SEA will give a better climate change impact assessment for the region.

ACKNOWLEDGEMENT

The authors acknowledge the SA-OBS dataset and the data providers in the SACA&D project (http://sacad.

database.bmkg.go.id/). The First author thanks the Indonesia Endowment Fund for Education (LPDP) (S-353/LPDP.3/2019) for providing fund for his PhD research. The second author acknowledges the support of the Royal Netherlands Embassy in Jakarta, Indonesia, through a Joint Cooperation Programme between Dutch and Indonesian research institutes. The HighResMIP simulations were made available through the PRIMAVERA project, which received funding from the European Union's Horizon 2020 Research and Innovation Programme under grant agreement no. 641727, which also supported authors Malcolm John Roberts, Marie-Pierre Moine, Alessio Bellucci, Retish Senan, Etienne Tourigny and Dian Putrasahan. The tenth author also received funding from an innovation programme under the Marie Skłodowska-Curie grant agreement No. 748750 (SPFireSD project).

AUTHOR CONTRIBUTIONS

Gerard van der Schrier: Conceptualization; investigation; project administration; resources; supervision; writing – review and editing. **Gert-Jan Steeneveld:** Conceptualization; investigation; project administration; resources; supervision; writing – review and editing. **Ardhasena Sopaheluwakan:** Conceptualization; investigation; project administration; resources; supervision; writing – review and editing. **Albert Tank:** Conceptualization; project administration; resources; supervision. **Malcolm J. Roberts:** Resources; software. **Marie Moine:** Resources. **A. Bellucci:** Resources. **Retish Senan:** Resources. **E Tourigny:** Resources. **Dian Putrasahan:** Resources.

ORCID

Mugni Hadi Hariadi https://orcid.org/0000-0003-3617-1277
Gerard van der Schrier https://orcid.org/0000-0001-7395-8023
Gert-Jan Steeneveld https://orcid.org/0000-0002-5922-8179
Ardhasena Sopaheluwakan https://orcid.org/0000-0002-4532-854X
Albert Klein Tank https://orcid.org/0000-0002-6275-2406
Malcolm John Roberts https://orcid.org/0000-0001-6128-6979
Marie-Pierre Moine https://orcid.org/0000-0002-6618-7782
Alessio Bellucci https://orcid.org/0000-0003-3766-1921
Retish Senan https://orcid.org/0000-0003-1949-1893
Etienne Tourigny https://orcid.org/0000-0003-4628-1461

REFERENCES

Aldrian, E., Dümenil-Gates, L., Jacob, D., Podzun, R. and Gunawan, D. (2004) Long-term simulation of Indonesian rainfall with the MPI regional model. *Climate Dynamics*, 22(8), 795–814. https://doi.org/10.1007/s00382-004-0418-9.

Aldrian, E., Gates, L.D. and Widodo, F.H. (2007) Seasonal variability of indonesian rainfall in echam4 simulations and in the reanalyses: the role of ENSO. *Theoretical and Applied Climatology*, 87(1), 41–59. https://doi.org/10.1007/s00382-004-0483-0.

Aldrian, E., Sein, D., Jacob, D., Gates, L.D. and Podzun, R. (2005) Modelling Indonesian rainfall with a coupled regional model. *Climate Dynamics*, 25(1), 1–17. https://doi.org/10.1007/s00382-004-0483-0.

Aldrian, E. and Susanto, D. (2003) Identification of three dominant rainfall regions within Indonesia and their relationship to sea surface temperature. *International Journal of Climatology*, 23(12), 1435–1454. https://doi.org/10.1002/joc.950.

Amsal, F., Harsa, H., Sopaheluwakan, A., Linarka, U., Pradana, R. and Satyaningsih, R. (2019). Bias correction of daily precipitation from downscaled CMIP5 climate projections over the Indonesian region. *IOP Conference Series: Earth and Environmental Science*, volume 303, p. 012046. IOP Publishing.

Cherchi, A., Fogli, P.G., Lovato, T., Peano, D., Iovino, D., Gualdi, S., Masina, S., Scoccimarro, E., Materia, S., Bellucci, A. and Navarra, A. (2019) Global mean climate and main patterns of variability in the CMCC-CM2 coupled model. *Journal of Advances in Modeling Earth Systems*, 11(1), 185–209. https://doi.org/10.1029/2018MS001369.

Demory, M.-E., Berthou, S., Sørland, S.L., Roberts, M.J., Beyerle, U., Seddon, J., Haarsma, R., Schär, C., Christensen, O. B., Fealy, R., Fernandez, J., Nikulin, G., Peano, D., Putrasahan, D., Roberts, C.D., Steger, C., Teichmann, C. and Vautard, R. (2020) Can high-resolution GCMs reach the level of information provided by 12–50 km CORDEX RCMs in terms of daily precipitation distribution? *Geoscientific Model Development*, 2020, 1–33. https://doi.org/10.5194/gmd-2019-370.

Diong, J.-Y., Tangang, F. and Juneng, L. (2019) An objective definition of summer monsoon onset in the northwestern maritime continent. *International Journal of Climatology*, 39, 4313–4328. https://doi.org/10.1002/joc.6075.

Doi, T., Vecchi, G.A., Rosati, A.J. and Delworth, T.L. (2012) Biases in the Atlantic ITCZ in seasonal-interannual variations for a coarse- and a high-resolution coupled climate model. *Journal of Climate*, 25(16), 5494–5511. https://doi.org/10.1175/JCLI-D-11-00360.1.

Emanuel, K.A. and Živković-Rothman, M. (1999) Development and evaluation of a convection scheme for use in climate models. *Journal of the Atmospheric Sciences*, 56(11), 1766–1782. https://doi.org/10.1175/1520-0469(1999)056¡1766:DAEOAC¿2.0.CO;2.

Funk, C., Peterson, P., Landsfeld, M., Pedreros, D., Verdin, J., Shukla, S., Husak, G., Rowland, J., Harrison, L., Hoell, A. and Michaelsen, J. (2015) The climate hazards infrared precipitation with stations—a new environmental record for monitoring extremes. *Scientific Data*, 2, 150066. https://doi.org/10.1038/sdata.2015.66.

Ge, F., Peng, T., Fraedrich, K., Sielmann, F., Zhu, X., Zhi, X., Liu, X., Tang, W. and Zhao, P. (2019) Assessment of trends and variability in surface air temperature on multiple high-resolution datasets over the Indochina Peninsula. *Theoretical*

and Applied Climatology, 135(3–4), 1609–1627. https://doi.org/10.1007/s00704-018-2457-x.

Giorgi, F., Coppola, E., Solmon, F., Mariotti, L., Sylla, M., Bi, X., Elguindi, N., Diro, G., Nair, V., Giuliani, G., Turuncoglu, U.U., Cozzini, S., Güttler, I., O'Brien, T.A., Tawfik, A.B., Shalaby, A., Zakey, A.S., Steiner, A.L., Stordal, F., Sloan, L.C. and Brankovic, C. (2012) RegCM4: model description and preliminary tests over multiple CORDEX domains. *Climate Research*, 52, 7–29. https://doi.org/10.3354/cr01018.

Gualdi, S., Alessandri, A. and Navarra, A. (2005) Impact of atmospheric horizontal resolution on El Nino Southern Oscillation forecasts. *Tellus A: Dynamic Meteorology and Oceanography*, 57(3), 357–374. https://doi.org/10.3402/tellusa.v57i3.14662.

Haarsma, R.J., Acosta, M., Bakhshi, R., Bretonnière, P.-A.B., Caron, L.-P., Castrillo, M., Corti, S., Davini, P., Exarchou, E., Fabiano, F., Fladrich, U., Fuentes Franco, R., García-Serrano, J., von Hardenberg, J., Koenigk, T., Levine, X., Meccia, V., van Noije, T., van den Oord, G., Palmeiro, F.M., Rodrigo, M., Ruprich-Robert, Y., Le Sager, P., Tourigny, E., Wang, S., van Weele, M. and Wyser, K. (2020) HighResMIP versions of EC-Earth: EC-Earth3P and EC-Earth3P-HR. Description, model performance, data handling and validation. *Geoscientific Model Development*, 2020, 1–37. https://doi.org/10.5194/gmd-2019-350.

Haarsma, R.J., Roberts, M.J., Vidale, P.L., Senior, C.A., Bellucci, A., Bao, Q., Chang, P., Corti, S., Fučkar, N.S., Guemas, V., Hardenberg, J.v., Hazeleger, W., Kodama, C., Koenigk, T., Leung, L.R., Lu, J., Luo, J.J., Mao, J., Mizielinski, M.S., Mizuta, R., Nobre, P., Satoh, M., Scoccimarro, E., Semmler, T., Small, J. and von Storch, J.S. (2016) High resolution model intercomparison project (HighResMIP v1. 0) for CMIP6. *Geoscientific Model Development*, 9(11), 4185–4208. https://doi.org/10.5194/gmd-9-4185-2016.

Hamada, J.-I., Yamanaka, M.D., Matsumoto, J., Fukao, S., Winarso, P.A. and Sribimawati, T. (2002) Spatial and temporal variations of the rainy season over Indonesia and their link to ENSO. *Journal of the Meteorological Society of Japan. Series II*, 80(2), 285–310. https://doi.org/10.2151/jmsj.80.285.

Juneng, L., Tangang, F., Chung, J.X., Ngai, S.T., Tay, T.W., Narisma, G., Cruz, F., Phan-Van, T., Ngo-Duc, T., Santisirisomboon, J., Singhruck, P., Gunawan, D. and Aldrian, E. (2016) Sensitivity of Southeast Asia rainfall simulations to cumulus and air-sea flux parameterizations in RegCM4. *Climate Research*, 69(1), 59–77. https://doi.org/10.3354/cr01386.

Liebmann, B., Camargo, S.J., Seth, A., Marengo, J.A., Carvalho, L. M., Allured, D., Fu, R. and Vera, C.S. (2007) Onset and end of the rainy season in South America in observations and the ECHAM 4.5 atmospheric general circulation model. *Journal of Climate*, 20(10), 2037–2050. https://doi.org/10.1175/JCLI4122.1.

Lintner, B.R., Biasutti, M., Diffenbaugh, N.S., Lee, J.-E., Niznik, M. J. and Findell, K.L. (2012) Amplification of wet and dry month occurrence over tropical land regions in response to global warming. *Journal of Geophysical Research: Atmospheres*, 117 (D11106), 1–10. https://doi.org/10.1029/2012JD017499.

Marjuki, Van der Schrier, G., Klein Tank, A.M.G., van den Besselaar, E.J.M., Nurhayati and Swarinoto, Y.S. (2016) Observed trends and variability in climate indices relevant for crop yields in Southeast Asia. *Journal of Climate*, 29(7), 2651–2669. https://doi.org/10.1175/JCLI-D-14-00574.1.

Masson, S., Terray, P., Madec, G., Luo, J.-J., Yamagata, T. and Takahashi, K. (2012) Impact of intra-daily SST variability on ENSO characteristics in a coupled model. *Climate Dynamics*, 39(3-4), 681–707. https://doi.org/10.1007/s00382-011-1247-2.

Moron, V., Robertson, A.W. and Boer, R. (2009) Spatial coherence and seasonal predictability of monsoon onset over Indonesia. *Journal of Climate*, 22(3), 840–850. https://doi.org/10.1175/2008JCLI2435.1.

Müller, W.A., Jungclaus, J.H., Mauritsen, T., Baehr, J., Bittner, M., Budich, R., Bunzel, F., Esch, M., Ghosh, R., Haak, H., Ilyina, T., Kleine, T., Kornblueh, L., Li, H., Modali, K., Notz, D., Pohlmann, H., Roeckner, E., Stemmler, I., Tian, F. and Marotzke, J. (2018) A higher-resolution version of the Max Planck Institute Earth System Model (MPI-ESM1. 2-HR). *Journal of Advances in Modeling Earth Systems*, 10(7), 1383–1413.

Naylor, R., Falcon, W., Wada, N. and Rochberg, D. (2002) Using El Niño-Southern Oscillation climate data to improve food policy planning in Indonesia. *Bulletin of Indonesian Economic Studies*, 38(1), 75–91. https://doi.org/10.1080/00074910275362093.

Ngo-Duc, T., Tangang, F.T., Santisirisomboon, J., Cruz, F., Trinh-Tuan, L., Nguyen-Xuan, T., Phan-Van, T., Juneng, L., Narisma, G., Singhruck, P., Gunawan, D. and Aldrian, E. (2017) Performance evaluation of RegCM4 in simulating extreme rainfall and temperature indices over the CORDEX-Southeast Asia region. *International Journal of Climatology*, 37(3), 1634–1647. https://doi.org/10.1002/joc.4803.

Nguyen-Thi, T., Ngo-Duc, T., Tangang, F.T., Cruz, F., Juneng, L., Santisirisomboon, J., Aldrian, E., Phan-Van, T. and Narisma, G. (2021) Climate analogue and future appearance of novel climate in southeast Asia. *International Journal of Climatology*, 41, E392–E409. https://doi.org/10.1002/joc.6693.

Nieuwolt, S. (1977) *Tropical Climatology: An Introduction to the Climates of the Low Latitudes*. London: John Wiley and Sons.

NOAA (2020). *Oceanic Niño Index Data*. National Climatic Data Center, National Oceanic and Atmospheric Administration.

Raäisaänen, J. (2007) How reliable are climate models. *Tellus A: Dynamic Meteorology and Oceanography*, 59(1), 2–29. https://doi.org/10.1111/j.1600-0870.2006.00211.x.

Randall, D.A., Wood, R.A., Bony, S., Colman, R., Fichefet, T., Fyfe, J., Kattsov, V., Pitman, A., Shukla, J., Srinivasan, J., Stouffer, R.J., Sumi, A. and Taylor, K.E. (2007). Climate Models and Their Evaluation. In: Solomon, S., D. Qin, M. Manning, Z. Chen, M. Marquis, K.B. Averyt, M.Tignor and H.L. Miller (eds.). Climate Change 2007: The Physical Science Basis. Contribution of Working Group I to the Fourth Assessment Report of the Intergovernmental Panel on Climate Change. Cambridge University Press, Cambridge, United Kingdom and New York, NY, USA.

Roberts, C.D., Senan, R., Molteni, F., Boussetta, S., Mayer, M. and Keeley, S.P. (2018) Climate model configurations of the ECMWF Integrated Forecasting System (ECMWF-IFS cycle 43r1) for HighResMIP. *Geoscientific Model Development*, 11(9), 3681–3712. https://doi.org/10.5194/gmd-2018-90.

Roberts, M.J., Baker, A., Blockley, E.W., Calvert, D., Coward, A., Hewitt, H.T., Jackson, L.C., Kuhlbrodt, T., Mathiot, P., Roberts, C.D., Schiemann, R., Seddon, J., Vannière, B. and Vidale, P.L. (2019) Description of the resolution hierarchy of the global coupled HadGEM3-GC3. 1 model as used in CMIP6 HighResMIP experiments. *Geoscientific Model Development*, 12(12), 4999–5028. https://doi.org/10.5194/gmd-12-4999-2019.

Seager, R., Naik, N. and Vogel, L. (2012) Does global warming cause intensified interannual hydroclimate variability. *Journal of Climate*, 25(9), 3355–3372. https://doi.org/10.1175/JCLI-D-11-00363.1.

Shaffrey, L., Stevens, I., Norton, W., Roberts, M., Vidale, P.-L., Harle, J., Jrrar, A., Stevens, D., Woodage, M.J., Demory, M.-E., Donners, J., Clark, D.B., Clayton, A., Cole, J.W., Wilson, S.S., Connolley, W.M., Davies, T.M., Iwi, A.M., Johns, T.C., King, J.C. A., New, A.L., Slingo, J.M., Slingo, A., Steenman-Clark, L. and Martin, G.M. (2009) U.K. HiGEM: The New U.K. High-Resolution Global Environment Model—Model Description and Basic Evaluation. *Journal of Climate*, 22(8), 1861–1896. https://doi.org/10.1175/2008JCLI2508.1.

Singh, V. and Xiaosheng, Q. (2019) Data assimilation for constructing long-term gridded daily rainfall time series over Southeast Asia. *Climate Dynamics*, 53, 1–25. https://doi.org/10.1007/s00382-019-04703-6.

Skamarock, W. C., Klemp, J. B., Dudhia, J., Gill, D. O., Barker, D. M., Duda, M. G., Yu Huang, X., Wang, W., and Powers, J. G. (2008). G.: A description of the Advanced Research WRF version 3. *NCAR Tech. Note NCAR/TN-475+STR*.

Sterl, A., van Oldenborgh, G.J., Hazeleger, W. and Burgers, G. (2007) On the robustness of ENSO teleconnections. *Climate Dynamics*, 29(5), 469–485. https://doi.org/10.1007/s00382-007-0251-z.

Supari, F.T., Juneng, L., Faye, C., Jing Xiang, C., Sheau Tieh, N., Ester, S., Mohd, S.F.M., Jerasorn, S., Patama, S., Tan, P., Ngo-Duc, T., Gemma, N., Edvin, A., Dodo, G. and Ardhasena, S. (2020) Multi-model projections of precipitation extremes in southeast Asia based on CORDEX-southeast Asia simulations. *Environmental Research*, 184, 109350. https://doi.org/10.1016/j.envres.2020.109350.

Tangang, F., Chung, J.X., Juneng, L., Salimun, E., Ngai, S.T., Jamaluddin, A.F., Mohd, M.S.F., Cruz, F., Narisma, G., Santisirisomboon, J., NgoDuc, T., Tan, P.V., Singhruck, P., Gunawan, D., Aldrian, E., Sopaheluwakan, A., Grigory, N., Remedio, A.R.C., Sein, D.V., HeinGriggs, D., McGregor, J.L., Yang, H., Sasaki, H. and Kumar, P. (2020) Projected future changes in rainfall in Southeast Asia based on CORDEX–sea multi-model simulations. *Climate Dynamics*, 55, 1247–1267.

Trouet, V. and Van Oldenborgh, G.J. (2013) KNMI climate explorer: a web-based research tool for high-resolution paleoclimatology. *Tree-Ring Research*, 69(1), 3–13. https://doi.org/10.3959/1536-1098-69.1.3.

Ul Hasson, S., Pascale, S., Lucarini, V. and Böhner, J. (2016) Seasonal cycle of precipitation over major river basins in South and Southeast Asia: a review of the CMIP5 climate models data for present climate and future climate projections. *Atmospheric Research*, 180, 42–63. https://doi.org/10.1016/j.atmosres.2016.05.008.

Van den Besselaar, E.J., Van der Schrier, G., Cornes, R.C., Iqbal, A.S. and Klein Tank, A.M. (2017) SA-OBS: a daily gridded surface temperature and precipitation dataset for Southeast Asia. *Journal of Climate*, 30(14), 5151–5165. https://doi.org/10.1175/JCLI-D-16-0575.1.

Van den Besselaar, E.J.M., Klein Tank, A.M.G., van der Schrier, G., Abass, M.S., Baddour, O., Cali, C., van Engelen, A.F.V., Freire, A., Hechler, P., Imbang Laksono, B., Iqbal, I., Jilderda, R., Kamga Foamouhoue, A., Kattenberg, A., Leander, R., Martínez Güingla, R., Mhanda, A.S., Nieto, J.J., Sunaryo, H., Suwondo, A., Swarinoto, Y.S. and Verver, G. (2015) International Climate Assessment & Dataset (ICA&D): climate services across borders. *Bulletin of the American Meteorological Society*, 96(1), 16–21. https://doi.org/10.1175/BAMS-D-13-00249.1.

Voldoire, A., Saint-Martin, D., Sénési, S., Decharme, B., Alias, A., Chevallier, M., Colin, J., Guérémy, J.-F., Michou, M., Moine, M.-P., Nabat, P., Roehrig, R., Salas y Mélia, D., Séférian, R., Valcke, S., Beau, I., Belamari, S., Berthet, S., Cassou, C., Cattiaux, J., Deshayes, J., Douville, H., Ethé, C., Franchistéguy, L., Geoffroy, O., Lévy, C., Madec, G., Meurdesoif, Y., Msadek, R., Ribes, A., Sanchez-Gomez, E., Terray, L. and Waldman, R. (2019) Evaluation of CMIP6 DECK Experiments with CNRM-CM6-1. *Journal of Advances in Modeling Earth Systems*, 11(7), 2177–2213. https://doi.org/10.1029/2019MS001683.

Wang, B. (2006) *The Asian Monsoon*. New York, NY: Springer Science & Business Media, Praxis. 787.

Wati, T., Kusumaningtyas, S. and Aldrian, E. (2019) Study of season onset based on water requirement assessment. In: *IOP Conference Series: Earth and Environmental Science*, Vol. 299, 299, 012042. Beijing, China: IOP Publishing. https://doi.org/10.1088/1755-1315/299/1/012042.

Wilks, D.S. (2011) *Statistical Methods in the Atmospheric Sciences*, Vol. 100. London: Academic Press.

Wyrtki, K. (1961). *Scientific results of marine investigations of the south China sea and the gulf of Thailand 1959–1961*. NAGA Report, 2:195.

Yang, H. (2012). Revision of climate change by dynamic downscaling over the maritime continents. https://apcc21.org/study/reportView.do?&lang=en&bbsId=BBSMSTR_000000000002&nttId=3608 [Accessed 25th October 2021].

Yatagai, A., Arakawa, O., Kamiguchi, K., Kawamoto, H., Nodzu, M. I. and Hamada, A. (2009) A 44-year daily gridded precipitation dataset for Asia based on a dense network of rain gauges. *Sola*, 5, 137–140. https://doi.org/10.2151/sola.2009-035.

Yatagai, A., Kamiguchi, K., Arakawa, O., Hamada, A., Yasutomi, N. and Kitoh, A. (2012) APHRODITE: constructing a long-term daily gridded precipitation dataset for Asia based on a dense network of rain gauges. *Bulletin of the American Meteorological Society*, 93(9), 1401–1415. https://doi.org/10.1175/BAMS-D-11-00122.1.

Zeng, X. and Lu, E. (2004) Globally unified monsoon onset and retreat indexes. *Journal of Climate*, 17(11), 2241–2248. https://doi.org/10.1175/1520-0442(2004)017¡2241:GUMOAR¿2.0.CO;2.

SUPPORTING INFORMATION

Additional supporting information may be found in the online version of the article at the publisher's website.

How to cite this article: Hariadi, M. H., van der Schrier, G., Steeneveld, G.-J., Sopaheluwakan, A., Tank, A. K., Roberts, M. J., Moine, M.-P., Bellucci, A., Senan, R., Tourigny, E., & Putrasahan, D. (2022). Evaluation of onset, cessation and seasonal precipitation of the Southeast Asia rainy season in CMIP5 regional climate models and HighResMIP global climate models. *International Journal of Climatology*, *42*(5), 3007–3024. https://doi.org/10.1002/joc.7404